ACS APPLIED NANO MATERIALS

www.acsanm.org Article

Doped Plasmonic Zinc Oxide Nanoparticles with Near-Infrared Absorption for Antitumor Activity

Nathalia Cristina Rissi, Edson J. Comparetti, Bianca Martins Estevão, Valmor Roberto Mastelaro, and Valtencir Zucolotto*

Cite This: https://doi.org/10.1021/acsanm.1c02197 Read Online

ACCESS | Metrics & More | Article Recommendations | Supporting Information

ABSTRACT: Plasmonic nanoparticles (NPs) have been extensively investigated as active materials for application in the optoelectronics, photocatalysis, and electrochemistry fields. In particular, doped metal oxides have attracted significant interest because of their optical and electrical properties. In this study, we investigated the influence of aluminum, gallium, and indium on the doping process of zinc oxide (ZnO) NPs. Physicochemical characterization revealed that, upon doping, ZnO NPs exhibited enhanced optoelectronic properties, including absorption in the near-infrared region. Lattice defects, such as vacancies and interstitials in the ZnO NPs crystal lattice, were also introduced by doping, changing the optical properties, and generating emission in the green-yellow, blue-violet, and orange-red band regions. We also investigated the ability of the ZnO NPs to induce cell death in human tumor cell lines and in a healthy cell line in vitro.

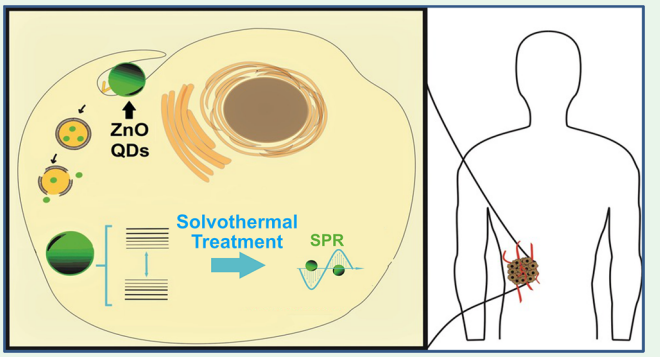

KEYWORDS: *plasmonic nanoparticles, ZnO QDs, ZnO nanorods, sol−gel synthesis, solvothermal treatment*

INTRODUCTION

The unique electronic properties of the plasmonic nanoparticles (NPs), including the surface plasmon resonance, have attracted attention in areas including optoelectronics, photocatalysis, and electrochemistry.[1,2] Doped metal oxides, in particular, have attracted attention because of their optical and electrical properties.[3,4] Among the oxide materials, zinc oxide (ZnO) is one of the most effective NPs for photovoltaics, catalysis, and sensing applications.[4,5]

The collective in-phase oscillation of electrons in NPs induces a dipole between the negative electron cloud and a positive core of the metal stimulated by incident light, an effect known as surface plasmon resonance (SPR).[6,7] The SPR in noble-metal NPs such as gold and silver nanoparticles (AuNPs and AgNPs) can be tuned by controlling their size and shape.[8] On the other hand, when it comes to ZnO, the SPR effect is influenced by the type of replacement metal, as well as the concentrations and synthetic routes employed. Aneesiya and Louis synthesized copper (Cu)-doped ZnO nanostructures via the coprecipitation method and obtained NPs with plasmonic bands between 500 and 800 nm depending on the molar concentration of Cu.[9] Vallejo et al., on the other hand, synthesized Cu- and cobalt (Co)-doped ZnO NPs for application in the degradation of methylene blue. The synthesis was performed by the sol−gel method, resulting in better dispersed NPs with a plasmonic band at 650 nm.[10] Sutka et al. reported the solvothermal synthesis of ZnO doped with Co and Ga, resulting in a magnetic NP with a plasmonic band in the IR region.[11] In this sense, the doping procedure is the most important parameter to be controlled for the creation of metallic conductivity in semiconductors.[12] Plasmonic semiconductor ZnO NPs may be obtained by the substitution of zinc (Zn) or oxygen (O) atoms in a process known as n-type (extra electrons) or p-type (extra holes) doping. n-type doping is most commonly used in plasmonic semiconductors, which represents the addition of one more valence electrons to the host crystal lattice, capable of tuning the optoelectronic properties of the semiconductor.[13] For ZnO NPs, n-type doping is usually achieved using aluminum (Al), gallium (Ga), or indium (In), providing electrical conductivity and SPR bands in the IR spectrum, remaining transparent in the visible region.[4,5,14]

Fluorescent ZnO quantum dots (QDs) have been used in the diagnostics of cancer cells upon imaging fluorescence using a continuous-wave laser.[15] In vivo studies have shown an

Received: July 28, 2021
Accepted: August 30, 2021

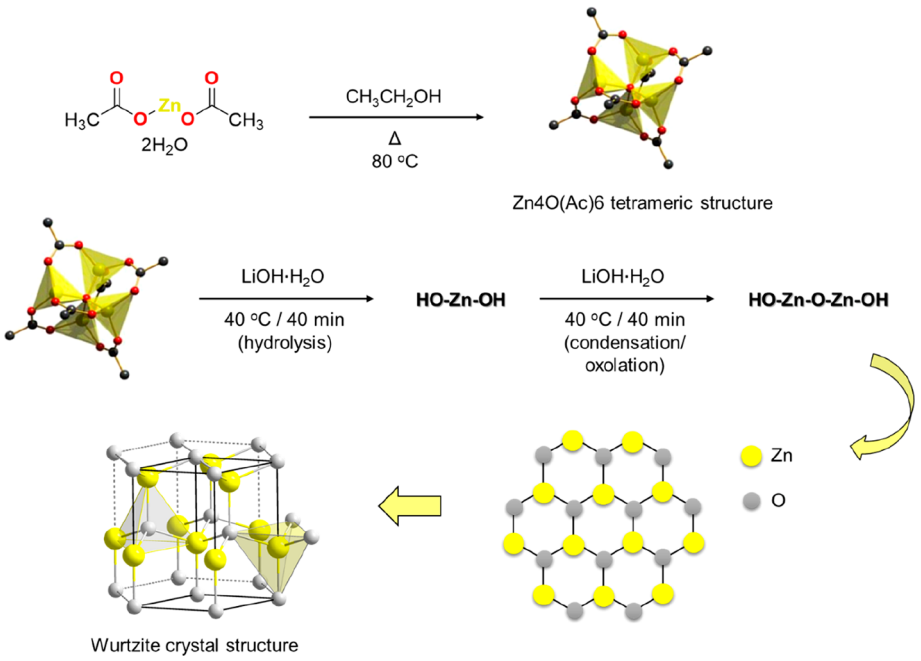

Figure 1. Schematic representation of the sol−gel synthesis of ZnO QDs.

excellent ability of the ZnO QDs to deliver doxorubicin and 5-fluorouracil in the tumor microenvironment of neoplasms.[15,16] In fact, ZnO nanocarriers increase the chemotherapeutics efficiency and cell death in cervical, breast, and lung cancer, with low cytotoxic effects in healthy cells.[16−18]

In this paper, we report a new two-stage synthetic route for the fabrication of high-quality plasmonic-doped ZnO NPs. In the first stage, the growth of ZnO QDs was controlled by time and temperature in the sol−gel synthesis, thus avoiding the formation of fractal aggregates in high temperatures and, consequently, the quenching of luminescence. In the second stage, ZnO QDs were treated at high temperature and pressure (solvothermal treatment), replacing the Zn^{2+} ions by the dopant atoms in the host crystal lattice, which changes their size and morphology and, consequently, their optoelectronic properties, resulting in plasmonic-doped ZnO NPs.[19] Finally, we investigate the cell viability of colorectal carcinoma cells (HTC-116) and healthy hepatic cells (HEPA-RG) to determine the appropriate concentration of ZnO NPs for future drug-delivery studies. Our results show that pure ZnO NPs and high concentrations of ZnO NPs doped with Al and Ga (80−100 ug/mL) impaired the proliferation of colon cancer cells during the period of 24 h without effects in healthy hepatic cells.

EXPERIMENTAL SECTION

ZnO NP Synthesis and Characterization. Initially, the zinc oxyacetate precursor was prepared using a well-established method proposed by Spanhel and Anderson.[20] The $Zn_{4O}(Ac)_6$ tetrameric precursor (herein referred to as the ZnAc precursor) was first prepared from an ethanolic dispersion (Synth, Brazil) by refluxing the solution containing 0.05 M $ZnAc_2{\cdot}2H_2O$ (Sigma-Aldrich, Brazil) for 2 h at 80 °C. In the following, the precursor was cooled to room temperature and stored at −10 °C. The doped ZnO QDs were synthesized in an ethanolic medium by the sol−gel method. First, the ZnAc precursor was added to the Al. The Ga and In [$Al(NO_3)_3{\cdot}9H_2O$, $Ga(NO_3)_3{\cdot}xH_2O$, and $In(NO_3)_3{\cdot}xH_20$, all purchased from Sigma-Aldrich, Brazil] dopants and hydrolysis and condensation reactions occurred under basic catalysis ($LiOH{\cdot}H_2O$, 98%, Vetec, Brazil) at 0.5 M, which was added under magnetic stirring at 40 °C and for 40 min. The concentrations of the dopants ranged from 2.5 to 20% compared to Zn^{2+}.

The solvothermal treatment of doped NPs was performed using a modified methodology proposed by Cimitan et al.[21] The synthetic route employed here was carried out by synthesizing the doped QDs, which were then inserted into a reaction autoclave in which the temperature and time were varied. Briefly, 100 mL of the QDs suspension was transferred into a Teflon-lined stainless-steel autoclave. The autoclave was sealed, and the treatment conditions were varied in terms of the temperature (150−200 °C) and time (8−18 h). The powders obtained after the solvothermal treatment were centrifuged, washed with distilled water and ethanol several times, and finally dried in a vacuum at 60 °C for 4 h.

Absorption spectra of the ZnO QDs suspensions in ethanol were measured using a UV−vis spectrophotometer (Hitachi U-2900). Diffuse-reflectance (DR-UV−vis) UV−vis spectra were recorded on a PerkinElmer Lambda 900 with a spectrometer equipped with a diffuse reflectance sphere. X-ray diffraction (XRD) patterns were obtained using a Bruker D8 Advanced diffractometer with Cu Kα radiation (λ = 1.54062 Å). High-resolution transmission electron microscopy (HR-TEM) images were collected in a JEM 2100 JEOL microscope operating at 200 kV. Scanning electron microscopy (SEM) was performed using an Zeiss SEM microscope equipped with a field emission gun (SEM-FEG). Fourier transform infrared (FTIR) spectroscopy was performed in a Nicolet 6700/GRAMS Suite equipment at 4000−400 cm^{-1}. ζ-potential measurements were performed at 25 °C with ZnO NPs dispersed in aqueous solution using a Malvern Zetasizer Nano-ZS equipment, which uses a 4 mW He−Ne laser operating at 633 nm at an angle of detection of 173°. For ζ-potential analyses, the suspensions at 10 $\mu g\ mL^{-1}$ of each material were prepared in deionized water and the culture medium Dulbecco's modified Eagle medium (DMEM) and measured immediately after 15 min of sonication. Photoluminescence (PL) spectra were measured in a Jobin Yvon Fluorolog spectrofluorimeter, under excitation from a xenon lamp. IR spectra of KBr pellets (1 mg sample to 80 mg KBr) were collected using a Nicolet 6700/GRAMS Suite spectrometer, with a resolution of 3 cm^{-1} and 128 scans. X-ray photoelectron spectroscopy (XPS) measurements were performed on an ESCA+ SCIENTA OMICRON spectrometer using monochromatic Al Kα (1486.6 eV) radiation. The high-resolution XPS spectra were recorded at a constant pass energy of 20 eV with 0.05 eV $step^{-1}$.

https://doi.org/10.1021/acsanm.1c02197
ACS Appl. Nano Mater. XXXX, XXX, XXX−XXX

Table 1. Average Particle Size of ZnO QDs ($2r$) Calculated from Equation 1

	excitonic peak (nm)	size (nm)		excitonic peak (nm)	size (nm)		excitonic peak (nm)	size (nm)
ZnO:Al 2.5%	3.65	2.98 ± 0.12	ZnO:Ga 2.5%	3.69	3.47 ± 0.10	ZnO:In 2.5%	3.66	3.00 ± 0.07
ZnO:Al 5%	3.63	2.83 ± 0.09	ZnO:Ga 5%	3.69	3.47 ± 0.15	ZnO:In 5%	3.63	2.82 ± 0.13
ZnO:Al 10%	3.61	2.68 ± 0.23	ZnO:Ga 10%	3.66	3.00 ± 0.22	ZnO:In 10%	3.60	2.62 ± 0.26
ZnO:Al 20%	3.61	2.68 ± 0.18	ZnO:Ga 20%	3.66	3.00 ± 0.31	ZnO:In 20%	3.58	2.51 ± 0.37

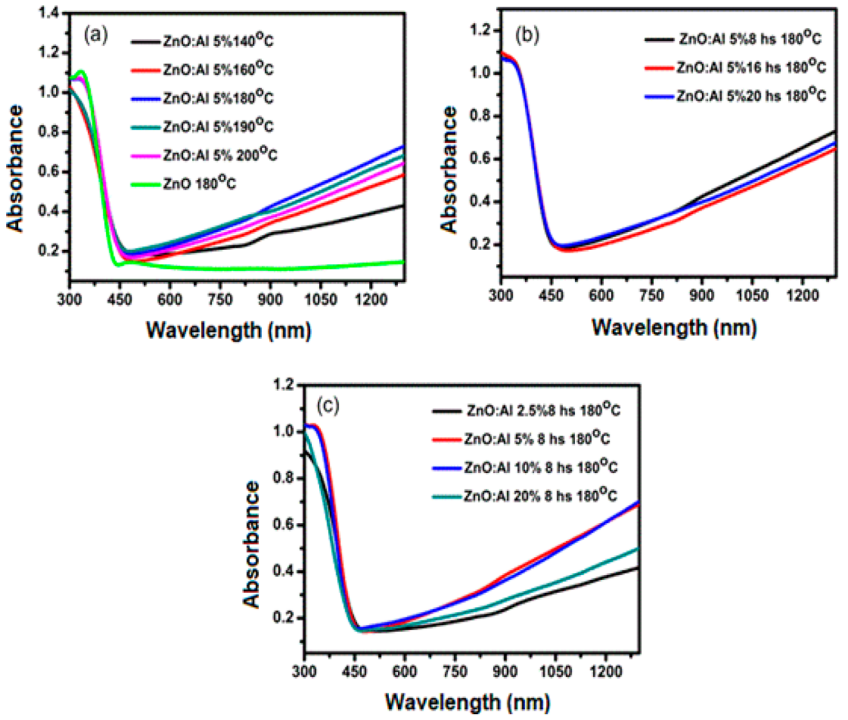

Figure 2. Optical absorption spectra (DR-UV−vis−NIR) of (a) doped ZnO NPs with 5% Al^{3+} treated at different temperatures for 8 h, (b) doped ZnO NPs with 5% Al^{3+} treated at different times (8, 15, and 18 h)/180 °C, and (c) doped ZnO NPs with 2.5, 5, 10, and 20% $[Al^{3+}]/[Zn^{2+}]$ at 180 °C/8 h.

A charge neutralizer (CN10) was used to exclude the surface charging effects. The binding energy of the spectra was corrected using the C 1s hydrocarbon component of the fixed value of 284.8 eV. The XPS data were analyzed using *CasaXPS* software (Casa Software Ltd., U.K.).

Cell Culture. HTC-116 and HEPA-RG were cultured in the complete medium [DMEM supplemented with 10% fetal bovine serum (FBS), 1% sodium pyruvate, 1% nonessential amino acids, 1% antibiotic and antimycotic (Life Technologies), and 4-(2-hydroxyethyl)-1-piperazineethanesulfonic acid (Sigma)] at 37 °C under a tension of 5% CO_2. Cells were detached from the plate surface using 0.05% trypsin−ethylenediaminetetraacetic acid (Gibco) for the following assays.

Cytotoxicity Analyses. Interaction of the NPs with the cells was analyzed by 3-(4,5-dimethylthiazol-2-yl)-2,5-diphenyltetrazolium bromide (MTT) colorimetric assays.[22] The MTT salt reduces to formazan crystals in mitochondrial metabolism, reflecting the activity of living cells as an indicator of the viability. The treatment was performed by adding the particles in a culture medium (1×10^4 cells $well^{-1}$), using a flat-bottom plate of 96 wells for 6 and 24 h. ZnO NPs (a), ZnO NPs doped with gallium (ZnO:Ga 5%) (b), ZnO NPs with aluminum (ZnO:Al 5%) (c), and ZnO NPs with indium (ZnO:In 5%) (d) were used as controls. As a positive control (maximal lysis), cells were exposed to dimethyl sulfoxide (DMSO). Cells were incubated in a solution of MTT for 3 h at 37 °C in 5% CO_2. The supernatant was then removed and the formazan crystals were solubilized with DMSO for further reading at 580 nm.

RESULTS AND DISCUSSION

The ZnO NPs synthesis via the sol−gel method starts with ZnO QDs nucleation and growth at the expense of zinc oxyacetate consumption by LiOH, forming small oligomers. In the following, aggregation of the oligomers leads to crystalline quartzite primary colloidal particles (Figure 1).[23] According to Caetano et al.,[24] primary particles aggregate and form a third type of colloidal particle with a multimodal size distribution of approximately 2 nm, which increases in size with time by a predominant aggregation mechanism. According to Zukoski and Bogush,[25] colloidal NPs are usually stabilized by steric/electrostatic repulsions, which prevents nucleation of the primary NPs. However, there are some kinetic parameters, including high temperatures, that directly influence the nucleation kinetics and can deplete the optoelectronic properties because of fast formation of the fractal aggregates.

The particle size and optical properties of doped ZnO QDs were investigated by UV−vis spectroscopy. The absorbance spectrum is capable of showing quantum confinement of the excitons in semiconductor NPs.[26] The method suggested by Nedelijković et al.[27] uses the intersection of peaks with the wavelength axis to determine the cutoff wavelength. ZnO QDs colloidal suspensions show a well-defined excitonic peak near 365 nm, typical for ZnO QDs. The wavelength limit (λ_c) is related to the energy of the band gap ($E_g = h_c/\lambda_c$). By using the

https://doi.org/10.1021/acsanm.1c02197
ACS Appl. Nano Mater. XXXX, XXX, XXX−XXX

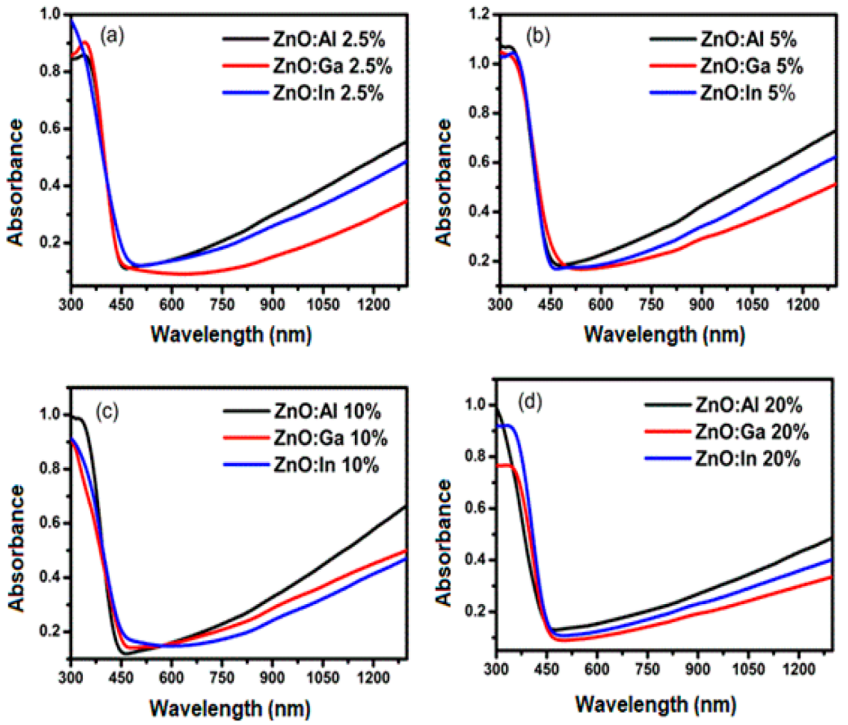

Figure 3. Optical absorption spectra (DR-UV−vis−NIR) of doped ZnO NPs with (a) 2.5% Al^{3+}, Ga^{3+}, and In^{3}, (b) 5% Al^{3+}, Ga^{3+}, and In^{3+}, (c) 10% Al^{3+}, Ga^{3+}, and In^{3+}, and (d) 20% Al^{3+}, Ga^{3+}, and In^{3+} treated for 8 h at 180 °C.

model proposed by Brus et al.,[28] it was possible to estimate the average size of the NPs. The model is based on confinement of the first excited electronic state, which can be approximated by eq 1:

$$E_g = E_g^{bulk} + \frac{h^2\pi^2}{2er^2}\left(\frac{1}{m_e{}^* m_0} + \frac{1}{m_h{}^* m_0}\right) - \frac{1.8e}{4\pi\varepsilon\varepsilon_0 r} - \frac{0.124e^3}{h^2(4\pi\varepsilon\varepsilon_0)^2}\left(\frac{1}{m_e{}^* m_0} + \frac{1}{m_h{}^* m_0}\right) - 1 \quad (1)$$

where E_g = 3.4 eV is the particle energy gap (bulk), h is the Plank constant; r is the particle radius, e is the electron charge, ε_0 is the vacuum permittivity, the relative permittivity ε = 3.7, m_e is the free electron mass, the effective electron mass $m_e{}^*$ = 0.24, and the effective hole mass $m_h{}^*$ = 0.45. The average particle size ($2r$) calculated from eq 1 is shown in Table 1.

Subsequently, the colloidal ZnO QDs suspension was transferred to a 100 mL Teflon-lined stainless-steel autoclave for solvothermal treatment. The solvothermal treatment conditions were varied according to the temperature (150−200 °C) and time (8−18 h). The precipitates were centrifuged, washed with ethanol, and dried at 60 °C. The influence of the temperature and time on the treatment of ZnO QDs was investigated using Al^{3+} ions. Al^{3+} is the best dopant element because of its small ionic radius and low cost. The substitution of Zn^{2+} ions with Al^{3+} in the crystal lattice is capable of increasing the electrical conductivity because of the increase of charge carriers into the NPs.[29,30]

According to Chen et al.,[31] parameters such as the temperature and time are capable of affecting the incorporation of the dopant in the lattice. The doping process is divided into four steps, namely, surface adsorption, lattice incorporation, lattice diffusion, and lattice ejection. However, it is energetically favorable that dopants be adsorbed only on the host surface instead of being incorporated into the semiconductor matrix.[32] In this latter case, control of the temperature is required for the dopants to be incorporated into the crystalline matrix of NPs.

The plasmonic properties of doped ZnO NPs with 5% Al^{3+} treated at different temperatures for 8 h were assessed by DR-UV−vis−NIR spectroscopy and are shown in Figure 2a (because of experimental limitations, the spectra had been collected in the range from 300 to 1300 nm, which is typically employed for these nanomaterials). Typical UV-absorption bands of ZnO NPs at about 310−350 nm can be seen for all samples. The spectra showed the plasmonic band by the influence of Al^{3+} ions, which can be clearly seen through strong absorption in the near-infrared (NIR) range (900 nm < λ < 1500 nm). It is possible to observe that an increase in the temperature (above 160 °C) leads to an appreciable increase in the NIR range.

Figure 2b shows the DR-UV−vis−NIR spectra of doped ZnO NPs with 5% Al^{3+} treated at different times (8, 15, and 18 h) at 180 °C. The samples presented no significant difference in terms of absorption; thus, 8 h of treatment was chosen for the next experiments. The spectra displayed the same typical UV-absorption bands of ZnO NPs at about 310−350 nm and absorption in the NIR range at 900 nm < λ < 1500 nm. Figure 2c shows the doped ZnO NPs with 2.5, 5, 10, and 20% [Al^{3+}]/[Zn^{2+}] at 180 °C/8 h. QDs containing 5% and 10% Al^{3+} showed the highest absorption in the NIR for λ > 900 nm. It is expected that the plasmonic band intensity of the NPs increases with the concentration and temperature. However, we observed a decrease in the band intensity above 160 °C, and with 20% [Al^{3+}]/[Zn^{2+}], there was also a decrease in the plasmonic band intensity. Melnikov et al. reported that the thermal stability of the $Al(NO_3)_3{\cdot}H_2O$ salt decreases above 160 °C, forming oxides and decreasing the doping.[33] In addition, Della Gaspera et al. noted that the increased

https://doi.org/10.1021/acsanm.1c02197
ACS Appl. Nano Mater. XXXX, XXX, XXX−XXX

concentration of the dopants provides a loss of crystallinity, decreasing the absorption intensity.[4]

To investigate the optoelectronic properties of ZnO NPs containing the dopants, different concentrations of Al^{3+} with other cations (Ga^{3+} and In^{3+}) were compared (all treated at 8 h/180 °C). Figure 3a shows the DR-UV−vis−NIR spectra of doped ZnO NPs with 2.5% Al^{3+}, Ga^{3+}, and In^{3+}. The spectra show the typical UV-absorption bands of ZnO NPs at about 310−350 nm and absorption in the NIR range from 900 to 1500 nm, which was more intense for the sample containing Al^{3+}. Figure 3b shows the DR-UV−vis−NIR spectra of doped ZnO NPs (5% of dopants), which presented practically the same absorption intensity in the NIR range (between 900 and 1500 nm) for the samples containing Al^{3+} and In^{3+} and a lower absorption intensity for Ga^{3+}. Figure 3c shows the DR-UV−vis−NIR spectra of doped ZnO NPs doped with 10% Al^{3+}, Ga^{3+}, and In^{3+}. The sample containing Al^{3+} exhibited the highest absorption intensity in the NIR range. The DR-UV−vis−NIR spectra of doped ZnO NPs with 20% dopants (Figure 3d) show practically the same intensity in the NIR range for all of the samples and a typical UV-absorption band between 310 and 350 nm.

In contrast to the results obtained by Della Gaspera et al.,[4] in which the intensity of the plasmon band and the doping efficiency were higher for In > Ga > Al, our results demonstrated that the absorption in the NIR region (900−1500 nm) was higher for Al > In > Ga. An efficiency doping is related to the ionic radii of the trivalent cations [0.8 Å (In), 0.62 Å (Ga), and 0.535 Å (Al)] with an ionic radius of Zn^{2+} of 0.74. The similarity between the dopants and host cation size, in the case of Zn^{2+}, favors substitution in the lattice, promoting more efficient doping compared to the other cations. However, the highest absorption for doped ZnO NPs with Al^{3+} (compared with In^{3+}) may be related to the solvothermal treatment of doped ZnO QDs, which may have increased the replacement of Al^{3+} ions in the crystalline lattice. After the optimization studies, we decided to use 5% concentration of the dopant metal, and a treatment temperature of 180 °C for 8 h, for all NPs.

Figure 4 shows the diffractograms of doped ZnO NPs at 5% with the different metals and nondoped ZnO NPs. The XRD peaks correspond to the diffraction planes from (100), (101), (102), (110), (103), and (200) of the ZnO NPs lattice, which is typical of the wurtzite phase.[17] The XRD peaks of nondoped ZnO NPs showed a strong orientation at (002), indicating that the growth pattern, in this case, is along the direction of the *c* axis, which represents the formation of ZnO nanorods.[34] The results are consistent with the TEM analyses. Both ZnO NPs and ZnO:Al exhibited the most elongated diffraction plane (002), thus presenting rod-shaped structures, which was less evident in Al doping. We observed a small-intensity inversion in the (110) and (103) planes, in which the (103) diffraction plane presented higher-intensity peaks in the ZnO nanorods, whereas for the doped nanorods, the peaks corresponding to the diffraction from the (110) plane are more intense. These small changes in the structural morphology can lead to ZnO nanorods with different formats, as can be observed in the TEM images. Also important to note is that the crystallinity was maintained even after doping.[4]

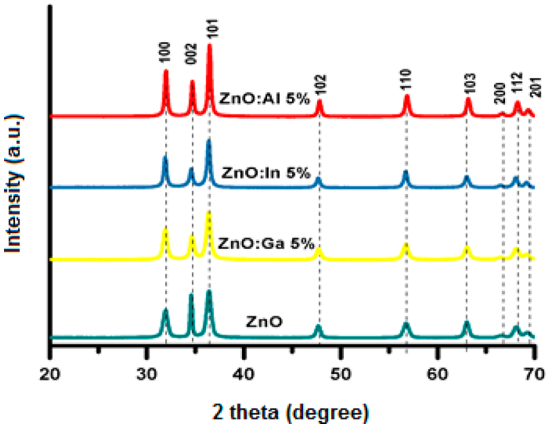

Figure 4. XRD patterns of ZnO NPs doped with 5% Al^{3+}, Ga^{3+}, and In^{3+} at 180 °C/8 h.

The NP morphology was investigated by TEM analysis, and the images are presented in Figure 5. The NPs exhibited

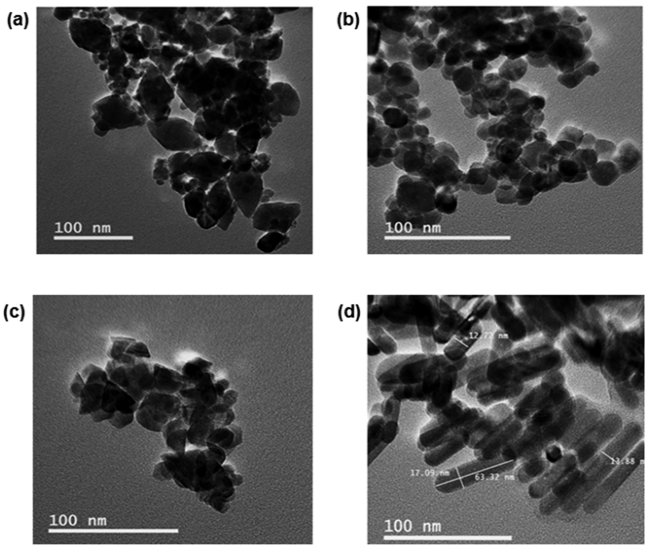

Figure 5. TEM images of ZnO NPs doped with 5% Al^{3+} (a), Ga^{3+} (b), and In^{3+} (c) and pure ZnO NPs (d) treated for 8 h at 180 °C.

different morphologies, such as spherical, angular, triangular, and nanorod. It can be seen that the NPs doped with 5% Al presented a mixed morphology with the predominance of angular shapes (slightly elongated) and average sizes in the range of 30 nm (as analyzed by the *ImageJ* software; Figure 5a).[35] Doping with 5% In also produced NPs of mixed morphology, with some triangular and hexagonal shapes and in the range of 25 nm (Figure 5b), similar to nanostructures reportd by Della Gaspera et al.[4] The doping with 5% Ga resulted in the predominance of spherical NPs with sizes in the 25 nm range (Figure 5c), as was also reported by Ghiloufi et al.[36]

It was also observed that the solvothermal treatment of nondoped NPs altered not only their crystalline properties but also their morphology, changing from spherical to nanorods (Figure 5d). This result corroborates the XRD data, which presented a longitudinal growth pattern toward the *c* axis. The nanorods were ca. 60 nm in length, with a diameter of 15 nm. Some papers have reported the formation of morphologically different NPs based on changes in the synthesis parameters, including the type of solvent and temperature, as well as in the absence/presence of base.[37,38] For example, Xu et al. investigated the effect of the organic solvent on the properties

https://doi.org/10.1021/acsanm.1c02197
ACS Appl. Nano Mater. XXXX, XXX, XXX−XXX

of ZnO NPs produced via a solvothermal method. ZnO NPs with different shapes including spheres, fibers, pyramids, and rods were obtained. In our study, because the same reagents and concentrations were employed in all syntheses, the differences in the particles' shape was probably driven by the presence of different dopant elements. However, a direct correlation between the differences in the NP shapes and their doping is not straightforward. It has been reported, for example, that noncrystalline regions may merge during the synthesis, leading to different NP morphologies.[39]

Figure 6 shows the emission spectra (PL) of bulk doped ZnO NPs (5% Al^{3+}, Ga^{3+}, or In^{3+}) and nondoped ZnO NPs,

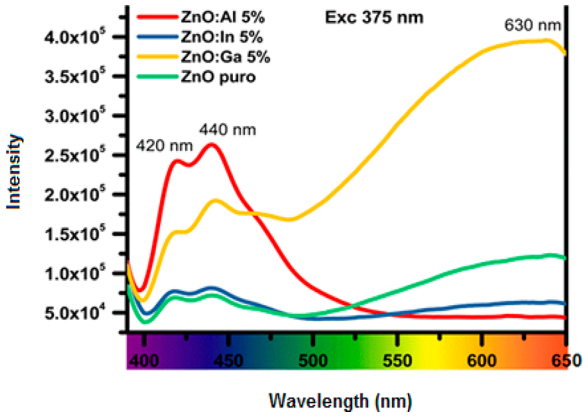

Figure 6. PL spectra of ZnO NPs doped with 5% Al^{3+} (a), Ga^{3+} (b), and In^{3+} (c) and pure ZnO NPs (d) treated for 8 h at 180 °C.

which were excited at 375 nm. It is important to observe that the emission at 630 nm (orange region) was higher for the ZnO:Ga sample. The emission at 420−440 nm (violet-blue range) was higher for the sample doped with Al^{3+}. The uncommon optical properties of the semiconductors in different wavelengths can be obtained by introducing defects in the ZnO NPs crystal lattice, during the synthesis process. According to Hou et al.,[40] in addition to intrinsic defects, the addition of dopants in the lattice determines its electrical and optical properties. The intrinsic defects can be vacancies or interstitial defects in the ZnO NPs crystal structure. The band emission in green-yellow is related to the oxygen vacancies (V_O),[41,42] the blue-violet emission is assigned to Zn interstitials (Zn_i) and Zn vacancies (V_{Zn}),[42,43] and the orange-red emission is related to the oxygen interstitials (O_i) or charged V_O.[44,45]

ζ-potential measurements were performed in ZnO NPs dispersed in water or a culture medium for evaluation of protein−corona formation on the particles' surface. In the former, xanthan gum was used as a dispersion agent. The average ζ potentials of doped ZnO NPs were estimated at −40.5 ± 0.8 mV (ZnO:Al 5%), −42.1 ± 1.0 mV (Zn:Ga 5%), −47.0 ± 0.9 mV (ZnO:In 5%), and −45.9 ± 0.9 mV (ZnO nanorods). The average ζ potentials for the dispersion of NPs in a culture medium with xanthan gum were −13.3 ± 0.9 mV (ZnO:Al 5%), −18 ± 1.0 mV (Zn:Ga 5%), −16.1 ± 0.9 mV (ZnO:In 5%), and −13.5 ± 0.8 mV (ZnO nanorods). The strongly negative ζ potentials for all of the samples are related to surface hydroxyl (OH) groups present on the NPs surface. The decrease in the ζ-potential values for the samples dispersed in the culture medium may be related to the formation of a protein corona because serum proteins dynamically associate with the particle surface.[46]

The synthesis of ZnO NPs by sol−gel is an interesting method because of its simplicity, low cost, and repeatability. However, the formation of acetates and other byproducts may occur during the process, which can bind or adsorb to the NPs.[20]

Figure 7 shows the IR spectra (FTIR) of NPs doped or not with 5% of the different metals. The presence of a broad

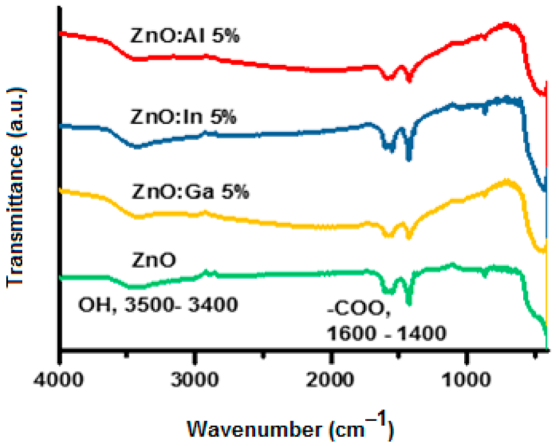

Figure 7. FTIR spectra of ZnO NPs doped with 5% Al^{3+}, Ga^{3+}, and In^{3+} and pure ZnO NPs treated for 8 h at 180 °C.

absorption band around 3400−3500 cm^{-1} is attributed to the hydroxyl stretch (OH−) vibrations. In the range of 1400−1600 cm^{-1}, the bands are attributed to the symmetrical and asymmetrical modes of the acetate group (COO−).[47−50]

XPS peak deconvolution of the doped ZnO NPs (Al, Ga, and In) and pure ZnO nanorods is shown in Figures S1−S4. The Zn 2p XPS peak (Figure S1A−D) has split spin−orbit components into $2p_{3/2}$ (1044.4 eV) and $2p_{1/2}$ (1021.3 eV) in $Zn_{51.4}O_{50.8}$ with an energy difference of 23 eV, indicating that the Zn atom in all of the samples is in the form of Zn^{2+}. The O 1s binding energy was deconvoluted into three peaks at approximately 530.3, 531.8, and 533.3 eV. The component at 530.3 eV corresponds to the O^{2-} ions inserted into the wurtzite structure. The binding energy at 531.8 eV can be attributed to O loosely adsorbed on the oxide surface and also to O^{2-} ions in the O-deficient regions within the ZnO NPs matrix (Figure S2a−d).[51] The ZnO nanorods and ZnO:Al and ZnO:Ga samples, but not the ZnO:In sample, exhibited a peak corresponding to the C═O bond, which refers to the synthesis of ZnO QDs, prepared by the refluxing of zinc acetate in ethanol. The Al 2p XPS spectra (Figure S3a−d) showed a single peak of the photoelectron at approximately 74 eV in $Zn_{41.5}O_{36.6}Al_{8.9}$, which corresponds to the Al^{3+} charge state. The binding energy of the Ga 2p levels was 117.7 and 1144.6 eV for Ga $2p_{3/2}$ and Ga $2p_{1/2}$ in $Zn_{45.5}O_{41.7}Ga_{2.7}$. According to Ramana et al.,[52] these binding energy values indicate that Ga is in the Ga^{3+} state. The XPS spectrum of In is also characterized by the two peaks with binding energies at 444.4 and 452 eV in $Zn_{42.3}O_{48.6}In_{9.1}$ that can be attributed to the state of In^{3+} (Figure S4a−c).[53] Therefore, XPS confirmed the results for DR-UV−vis−NIR and TEM, showing that doping with the respective metals occurred.

Some papers from the literature point to the cytotoxicity of ZnO, ZnO:Al, and ZnO:Mg NPs.[54,55] In a review paper, Pandurangan and Kim addressed the toxicity of ZnO against several cell lines, such as BEAS-2b (bronchial epithelial cells

https://doi.org/10.1021/acsanm.1c02197
ACS Appl. Nano Mater. XXXX, XXX, XXX−XXX

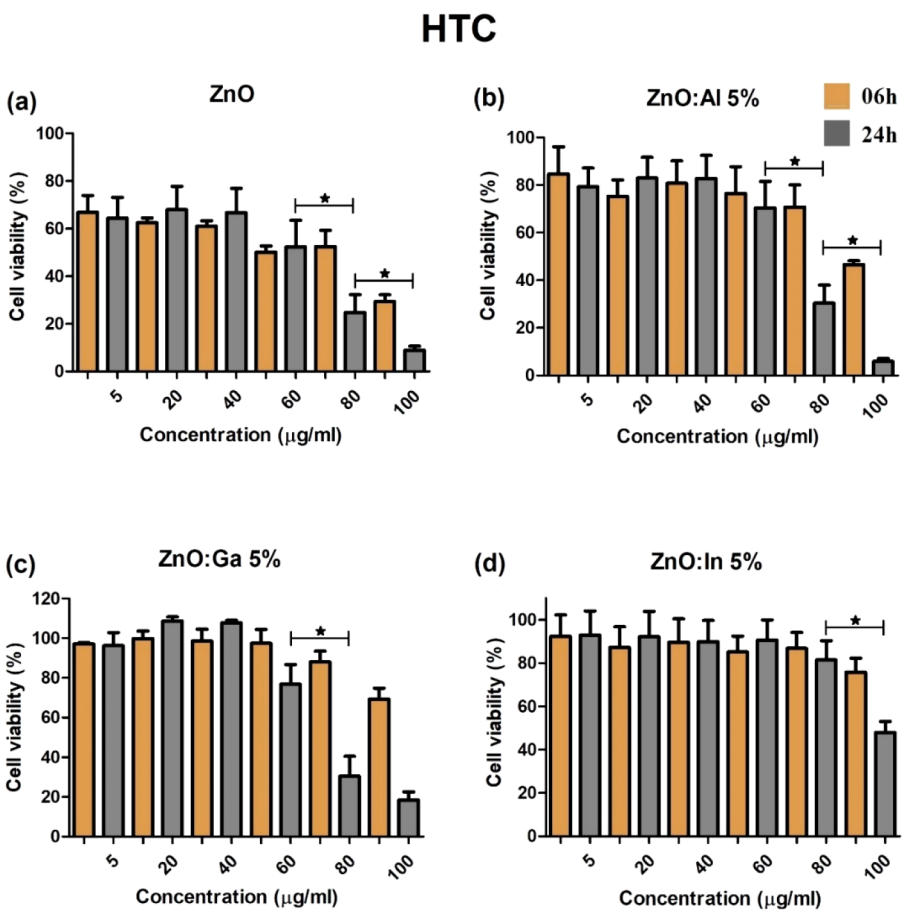

Figure 8. Cytotoxicity analysis of ZnO NPs in colon cancer cells (HCT-116) by methyltetrazolium reduction (MTT). HCT (1×10^5 cells well^{-1}) was exposed to (a) pure ZnO NPs, (b) ZnO NPs doped with Al^{3+} (ZnO:Al 5%), (c) ZnO NPs doped with Ga^{3+} (ZnO:Ga 5%), and (d) ZnO NPs doped with In^{3+} (ZnO:In 5%) to verify their toxicity in different concentrations of NPs (5−100 μg mL^{-1}) and after 6 and 24 h of incubation.

from a normal human lung), A549 (epithelial cells from human lung carcinoma), C2C12 (cell line from mouse muscle myoblast), 3T3-L1 (mouse embryonic fibroblast cell line), HaCaT (human keratinocytes), SK Mel-28 (human melanoma), RKO and Caco-2 (human colon carcinoma cell lines), H1355 (human lung carcinoma cells), HepG2 (human hepatocellular carcinoma cells), and LoVo (human colon carcinoma cells). Khashan et al. also investigated the toxicity of Al:ZnO using human triple-negative breast cancer (MDA-MB-231). However, studies based on doping with other metals are scarce.

We investigate the toxicity of ZnO NPs against HCT-116 and HEPA-RG because the literature reports a possible accumulation of ZnO NPs in the digestive tract,[56] in addition to the evaluation of possible toxicity in the liver, because this organ acts as a biological filtration system that retains 30−99% of administering NPs from the bloodstream.[57] In vitro tests were performed using ZnO NPs concentrations between 5 and 100 μg mL^{-1}. Pure ZnO NPs had the highest toxicity in all concentrations tested (5−100 μg mL^{-1}) compared to other experimental groups, in which we observed a reduction in the NP toxicity after the incorporation of metal elements, as shown in Figure 8a. ZnO NPs doped with Al^{3+}, Ga^{3+}, and In^{3+} were innocuous to tumor cells at concentrations below 60 μg mL^{-1}. After 24 h of incubation, only high doses (60−100 μg mL^{-1}) of doped NPs exhibited significant toxicity (Figure 8b−d).

Similar results were found by Wang et al.[58] and Pandurangan et al.,[59] who examined the cell viability and phenotypic changes after exposure with ZnO NPs in oral and cervical cancer cell lines. Unlike our findings, a high cytotoxicity of low doses of ZnO NPs (<30 μg/mL) after 24 h was observed. The concentration of the NPs tested here did not interfere in the cell viability, reinforcing our hypothesis that high doses of ZnO NPs can be safely manipulated to achieve antitumor activity because they present a lower risk for inducing tolerance. Therefore, metal elements loaded into ZnO NPs structures seem to inhibit activity and, in this case, reduce its cytotoxic potential because MTT assays indicated higher toxicity for pure samples. Murdock et al. reported that the presence of serum in the culture medium favors the dispersion and stability of oxide and metal NPs.[60] The authors also observed that the presence of proteins on the NPs' surface decreases the adhesion of NPs to cells, suggesting surface modification and decreasing the toxicity. In our studies, all NPs showed a significant decrease in the ζ potential in the presence of a culture medium and serum, indicating protein−corona formation. The differences in the toxicological effects, in this case, are intrinsically linked to the different chemical compositions of the NPs,[60] as well as the higher toxicity occurring at higher concentrations, because of the surface modification provided by the adsorbed proteins.[60]

Moon et al.[61] described the ZnO NPs ability to induce cell death as a consequence of reactive oxygen species (ROS) induced by Zn^+ ions. In cancer cells, ROS inhibited antiapoptotic molecules, like inhibitors of apoptosis proteins and hypoxia-inducible factor. However, ROS production

https://doi.org/10.1021/acsanm.1c02197
ACS Appl. Nano Mater. XXXX, XXX, XXX−XXX

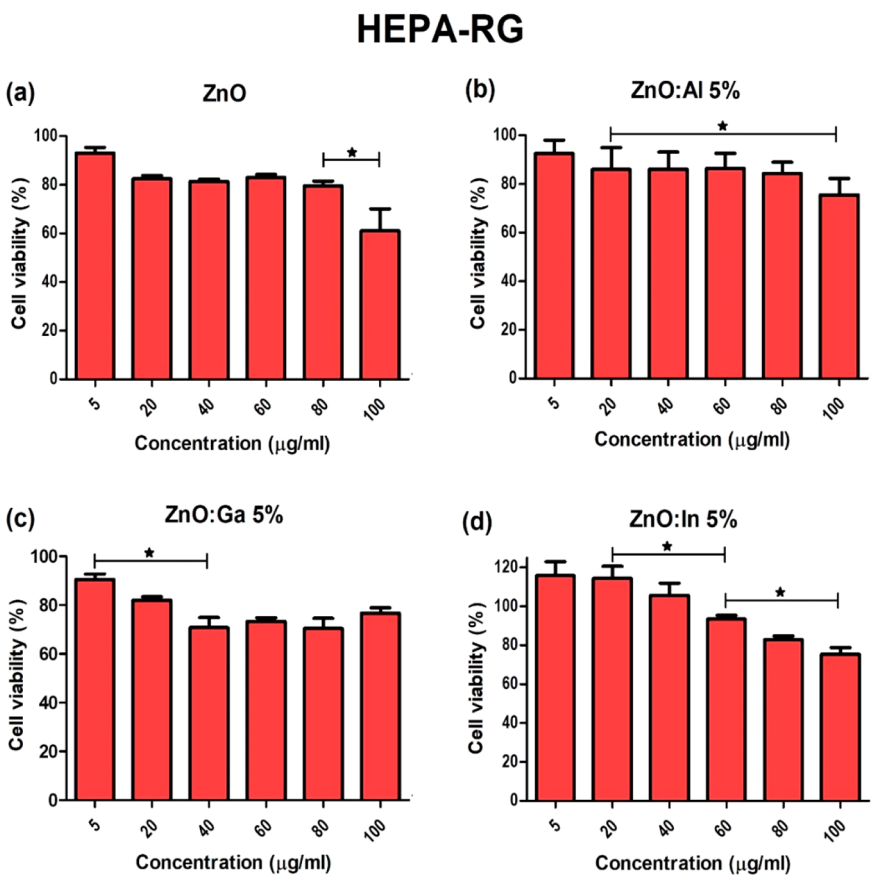

Figure 9. Cytotoxicity analysis of ZnO NPs in HEPA-RG by methyltetrazolium reduction (MTT). HEPA-REG (1×10^5 cells well^{-1}) was exposed to (a) pure ZnO NPs, (b) ZnO NPs doped with Al^{3+} (ZnO:Al 5%), (c) ZnO NPs doped with Ga^{3+} (ZnO:Ga 5%), and (d) ZnO NPs doped with In^{3+} (ZnO:In 5%) to verify their toxicity at different NP concentrations (5−100 μg mL^{-1}) during 24 h.

supported ZnO NPs migration through neoplasm cells in a 3D tumor cell culture, enhancing the apoptosis process in a cancer environment via caspase 3/7 activation.[61,62]

Because the NPs' size, shape, and surface functionalization influence their migration in the body, the so-called permeability and retention effect (EPR effect) aid the accumulation of structures with a molecular weight higher than 40 kDa in hypervascularized tissues (like lung, liver, kidneys, spleen, and tumor microenvironments).[63] The ZnO NPs described here increased the viability of HEPA-RG in all concentrations after 24 h of exposure (Figure 9). This is relevant because it is essential that nanocarriers can be captured by neoplastic cells easier than other cell lines in the organism.

In the body, white blood cells represent the first barrier to be overcome by nanomaterials.[64,65] Previous studies have shown that low concentrations of ZnO NPs in immature immunocompetent cells do not induce an alteration in functional responses and phenotypic changes but may act as antineoplastic agents, triggering antitumor activity in vitro and in vivo.[66] However, to advance in the clinical trials, a deep understanding of the NP cytotoxicity in other cell lines that constitutes the tumor environment, such as macrophages, lymphocytes, cancer-associated fibroblasts, and vascular endothelial cells, is required. In monocytes, ZnO NPs nanostructures have shown the ability to polarize macrophages to M1-like phenotype, inducing expression of costimulatory proteins (like MHC-II, CD80, and CD86) and production of proinflammatory cytokines.[62] Such properties could modulate tumor associate macrophages (TAMs) and restore a classical immune response in tumor sites. Unfortunately, the interaction between human activated T cells and ZnO NPs is more intense than that for unactivated cells, increasing myeloid cell death by ROS production.[67] Our results exhibit the feasibility for future conjugation of ZnO NPs with target molecules, favoring their internalization by specific cell lines to increase activity in neoplastic cell receptors. Here, ZnO NPs produced side effects in tumor cells (HCT-116), but at low concentrations, the conjugation with metals did not promote any increment in the cytotoxic activity, requiring further studies to adsorb antibodies or aptamers on the NPs' surface.

ZnO NPs represent an important class of nanocarriers that can be tailored for advanced drug delivery and cancer therapy because it has been reported by Puvvada et al. that used ZnO NPs for taxol delivery in human breast cancer cells in vitro and in vivo.[68] Hu et al. reported on a ZnO nanostructure combining graphene and folic acid for photodynamic therapy,[69] in which an increased specificity of the photodynamic therapy was achieved against cancer cells, reducing the cytotoxicity to normal tissues.[69] Beyond cancer therapy, ZnO NPs structures hold antibacterial activity after inducing ROS formation against Gram-positive and Gram-negative bacteria.[70] We believe that ZnO NPs are excellent structures to combine the usual treatments against chronic and infectious disease in a single therapeutic platform.

https://doi.org/10.1021/acsanm.1c02197
ACS Appl. Nano Mater. XXXX, XXX, XXX−XXX

CONCLUSIONS

We designed a new synthetic route for plasmonic-doped ZnO NPs with absorption in the NIR. We have controlled the kinetic growth of the NPs during the sol−gel process, avoiding the formation of compact aggregates, which may quench the luminescence of bulk ZnO NPs. The treatment of ZnO QDs using high temperature and pressure (solvothermal treatment) replaced the Zn^{2+} ions by dopant atoms into the host crystal lattice, promoting SPR. The plasmonic ZnO NPs-based semiconductors represent an alternative in the use of conventional metals, allowing their use as theranostic tools with a cheaper and large-scale synthesis. Furthermore, we anticipate the cytotoxic potential of doped ZnO NPs, which is important for their use in biological applications.

ASSOCIATED CONTENT

Supporting Information

The Supporting Information is available free of charge at https://pubs.acs.org/doi/10.1021/acsanm.1c02197.

XPS peak deconvolution of the doped ZnO NPs (Al, Ga, and In) and pure ZnO NPs, shown in Figures S1−S4 (PDF)

AUTHOR INFORMATION

Corresponding Author

Valtencir Zucolotto − *Nanomedicine and Nanotoxicology Group, São Carlos Institute of Physics, University of São Paulo, São Carlos 13566-590, Brazil; Institute of Advanced Studies, University of São Paulo, São Carlos 13566-590, Brazil;* orcid.org/0000-0003-4307-3077; Email: zuco@ifsc.usp.br

Authors

Nathalia Cristina Rissi − *Nanomedicine and Nanotoxicology Group, São Carlos Institute of Physics, University of São Paulo, São Carlos 13566-590, Brazil;* orcid.org/0000-0001-8993-2637

Edson J. Comparetti − *Nanomedicine and Nanotoxicology Group, São Carlos Institute of Physics, University of São Paulo, São Carlos 13566-590, Brazil*

Bianca Martins Estevão − *Nanomedicine and Nanotoxicology Group, São Carlos Institute of Physics, University of São Paulo, São Carlos 13566-590, Brazil;* orcid.org/0000-0001-7913-6979

Valmor Roberto Mastelaro − *Group of Nanomaterials and Advanced Ceramics, São Carlos Institute of Physics, University of São Paulo, São Carlos 13563-120, Brazil;* orcid.org/0000-0001-9512-4214

Complete contact information is available at: https://pubs.acs.org/10.1021/acsanm.1c02197

Author Contributions

The manuscript was written through contributions of all authors. All authors approved the final version of the manuscript.

Notes

The authors declare no competing financial interest.

ACKNOWLEDGMENTS

This study was funded by the Brazilian National Council for Scientific and Technological Development (Projects 153396/2018-0, 155451/2018-9, 309943/2020-5, and 442690/2020-7) and São Paulo Research Foundation (Projects 2018/12670-4, 2017/22056-9, and 2020/00124-5).

ABBREVIATIONS

AgNPs, silver nanoparticles
Al, aluminum
AuNPs, gold nanoparticles
DMEM, Dulbecco's modified Eagle medium
DMSO, dimethyl sulfoxide
DR-UV−vis, diffuse-reflectance UV−vis
EPR effect, retention effect
FTIR, Fourier transform infrared
Ga, gallium
HEPA-RG, hepatic stem cell line
HR-TEM, high-resolution transmission electron microscopy
HTC-116, human colorectal cancer cells
In, indium
λ_c, wavelength limit
FEG, field emission gun
MTT, 3-(4,5-dimethylthiazol-2-yl)-2,5-diphenyltetrazolium bromide
NPs, nanoparticles
PL, photoluminescence
QDs, quantum dots
ROS, reactive oxygen species
SPR, surface plasmon resonance
TAMs, tumor associate macrophages
XPS, X-ray photoelectron spectroscopy
XRD, X-ray diffraction
ZnO, zinc oxide

REFERENCES

(1) Lal, S.; Link, S.; Halas, N. J. Nano-Optics from Sensing to Waveguiding. *Nat. Photonics* **2007**, *1*, 641−648.
(2) Xie, T.; Jing, C.; Long, Y. T. Single Plasmonic Nanoparticles as Ultrasensitive Sensors. *Analyst* **2017**, *142* (3), 409−420.
(3) Lounis, S. D.; Runnerstrom, E. L.; Llordés, A.; Milliron, D. J. Defect Chemistry and Plasmon Physics of Colloidal Metal Oxide Nanocrystals. *J. Phys. Chem. Lett.* **2014**, *5* (9), 1564−1574.
(4) Della Gaspera, E.; Chesman, A. S. R.; Van Embden, J.; Jasieniak, J. J. Non-Injection Synthesis of Doped Zinc Oxide Plasmonic Nanocrystals. *ACS Nano* **2014**, *8* (9), 9154−9163.
(5) Della Gaspera, E.; Guglielmi, M.; Perotto, G.; Agnoli, S.; Granozzi, G.; Post, M. L.; Martucci, A. CO Optical Sensing Properties of Nanocrystalline ZnO-Au Films: Effect of Doping with Transition Metal Ions. *Sens. Actuators, B* **2012**, *161* (1), 675−683.
(6) Abadeer, N. S.; Murphy, C. J. Recent Progress in Cancer Thermal Therapy Using Gold Nanoparticles. *J. Phys. Chem. C* **2016**, *120* (9), 4691−4716.
(7) Govorov, A. O.; Richardson, H. H. Generating Heat with Metal Nanoparticles. *Nano Today* **2007**, *2* (1), 30−38.
(8) Kvítek, O.; Siegel, J.; Hnatowicz, V.; Švorčík, V. Noble Metal Nanostructures Influence of Structure and Environment on Their Optical Properties. *J. Nanomater.* **2013**, *2013*, 1.
(9) Aneesiya, K. R.; Louis, C. Localized Surface Plasmon Resonance of Cu-Doped ZnO Nanostructures and the Material's Integration in Dye Sensitized Solar Cells (DSSCs) Enabling High Open-Circuit Potentials. *J. Alloys Compd.* **2020**, *829*, 154497.
(10) Vallejo, W.; Cantillo, A.; Salazar, B.; Diaz-Uribe, C.; Ramos, W.; Romero, E.; Hurtado, M. Comparative Study of ZnO Thin Films Doped with Transition Metals (Cu and Co) for Methylene Blue Photodegradation under Visible Irradiation. *Catalysts* **2020**, *10* (5), 528.

(11) Šutka, A.; Käämbre, T.; Joost, U.; Kooser, K.; Kook, M.; Duarte, R. F.; Kisand, V.; Maiorov, M.; Döbelin, N.; Smits, K. Solvothermal Synthesis Derived Co-Ga Codoped ZnO Diluted Magnetic Degenerated Semiconductor Nanocrystals. *J. Alloys Compd.* **2018**, *763*, 164−172.
(12) Šutka, A.; Timusk, M.; Döbelin, N.; Pärna, R.; Visnapuu, M.; Joost, U.; Käämbre, T.; Kisand, V.; Saal, K.; Knite, M. A Straightforward and "Green" Solvothermal Synthesis of Al Doped Zinc Oxide Plasmonic Nanocrystals and Piezoresistive Elastomer Nanocomposite. *RSC Adv.* **2015**, *5* (78), 63846−63852.
(13) Luther, J. M.; Jain, P. K.; Ewers, T.; Alivisatos, A. P. Localized Surface Plasmon Resonances Arising from Free Carriers in Doped Quantum Dots. *Nat. Mater.* **2011**, *10* (5), 361−366.
(14) Khuili, M.; Fazouan, N.; El Makarim, H. A.; El Halani, G.; Atmani, E. H. Comparative First Principles Study of ZnO Doped with Group III Elements. *J. Alloys Compd.* **2016**, *688*, 368−375.
(15) Wang, L.; Cai, Y.; An, Z.; Gu, W.; Chen, P.; Cai, Q. ZnO-Functionalized Mesoporous Inner-Empty Nanotheranostic Platform: Upconversion Imaging Guided Chemotherapy with PH-Triggered Drug Delivery. *Nanotechnology* **2018**, *29* (50). 505101.
(16) Xiao, X.; Liang, S.; Zhao, Y.; Huang, D.; Xing, B.; Cheng, Z.; Lin, J. Core-Shell Structured 5-FU@ZIF-90@ZnO as a Biodegradable Nanoplatform for Synergistic Cancer Therapy. *Nanoscale* **2020**, *12* (6), 3846−3854.
(17) Raghavendra, A. J.; Gregory, W. E.; Slonecki, T. J.; Dong, Y.; Persaud, I.; Brown, J. M.; Bruce, T. F.; Podila, R. Three-Photon Imaging Using Defect-Induced Photoluminescence in Biocompatible ZnO Nanoparticles. *Int. J. Nanomed.* **2018**, *13*, 4283−4290.
(18) Zangeneh, M.; Nedaei, H. A.; Mozdarani, H.; Mahmoudzadeh, A.; Salimi, M. Enhanced Cytotoxic and Genotoxic Effects of Gadolinium-Doped ZnO Nanoparticles on Irradiated Lung Cancer Cells at Megavoltage Radiation Energies. *Mater. Sci. Eng., C* **2019**, *103*, 109739.
(19) Shanthi, S. I.; Poovaragan, S.; Arularasu, M. V.; Nithya, S.; Sundaram, R.; Magdalane, C. M.; Kaviyarasu, K.; Maaza, M. Optical, Magnetic and Photocatalytic Activity Studies of Li, Mg and Sr Doped and Undoped Zinc Oxide Nanoparticles. *J. Nanosci. Nanotechnol.* **2018**, *18* (8), 5441−5447.
(20) Spanhel, L.; Anderson, M. A. Semiconductor Clusters in the Sol-Gel Process: Quantized Aggregation, Gelation, and Crystal Growth in Concentrated ZnO Colloids. *J. Am. Chem. Soc.* **1991**, *113* (8), 2826−2833.
(21) Cimitan, S.; Albonetti, S.; Forni, L.; Peri, F.; Lazzari, D. Solvothermal Synthesis and Properties Control of Doped ZnO Nanoparticles. *J. Colloid Interface Sci.* **2009**, *329* (1), 73−80.
(22) Shenoy, N.; Stenson, M.; Lawson, J.; Abeykoon, J.; Patnaik, M.; Wu, X.; Witzig, T. Drugs with Anti-Oxidant Properties Can Interfere with Cell Viability Measurements by Assays That Rely on the Reducing Property of Viable Cells. *Lab. Invest.* **2017**, *97* (5), 494−497.
(23) Znaidi, L. Sol-Gel-Deposited ZnO Thin Films: A Review. *Mater. Sci. Eng., B* **2010**, *174* (1−3), 18−30.
(24) Caetano, B. L.; Santilli, C. V.; Meneau, F.; Briois, V.; Pulcinelli, S. H. In Situ and Simultaneous UV-Vis/SAXS and UV-Vis/XAFS Time-Resolved Monitoring of ZnO Quantum Dots Formation and Growth. *J. Phys. Chem. C* **2011**, *115* (11), 4404−4412.
(25) Bogush, G. H.; Zukoski, C. F. Uniform Silica Particle Precipitation: An Aggregative Growth Model. *J. Colloid Interface Sci.* **1991**, *142* (1), 19−34.
(26) Rossetti, R.; Brus, L. Electron-Hole Recombination Emission as a Probe of Surface Chemistry in Aqueous CdS Colloids. *J. Phys. Chem.* **1982**, *86* (23), 4470−4472.
(27) Nedelijković, J. M.; Patel, R. C.; Kaufman, P.; Joyce-Pruden, C.; O'Leary, N. Synthesis and Optical Properties of Quantum-Size Metal Sulfide Particles in Aqueous Solution. *J. Chem. Educ.* **1993**, *70* (4), 342−345.
(28) Brus, L. E. A Simple Model for the Ionization Potential, Electron Affinity, and Aqueous Redox Potentials of Small Semiconductor Crystallites. *J. Chem. Phys.* **1983**, *79* (11), 5566−5571.
(29) Özgür, Ü.; Alivov, Y. I.; Liu, C.; Teke, A.; Reshchikov, M. A.; Doğan, S.; Avrutin, V.; Cho, S. J.; Morkoc, H. A Comprehensive Review of ZnO Materials and Devices. *J. Appl. Phys.* **2005**, *98* (4), 041301.
(30) Minami, T. Transparent Conducting Oxide Semiconductors for Transparent Electrodes. *Semicond. Sci. Technol.* **2005**, *20* (4), S35.
(31) Chen, D.; Viswanatha, R.; Ong, G. L.; Xie, R.; Balasubramaninan, M.; Peng, X. Temperature Dependence of "Elementary Processes" in Doping Semiconductor Nanocrystals. *J. Am. Chem. Soc.* **2009**, *131* (26), 9333−9339.
(32) Zheng, W.; Wang, Z.; Wright, J.; Goundie, B.; Dalal, N. S.; Meulenberg, R. W.; Strouse, G. F. Probing the Local Site Environments in Mn:CdSe Quantum Dots. *J. Phys. Chem. C* **2011**, *115* (47), 23305−23314.
(33) Melnikov, P.; Nascimento, V. A.; Arkhangelsky, I. V.; Zanoni Consolo, L. Z. Thermal Decomposition Mechanism of Aluminum Nitrate Octahydrate and Characterization of Intermediate Products by the Technique of Computerized Modeling. *J. Therm. Anal. Calorim.* **2013**, *111* (1), 543−548.
(34) Tang, Z. R.; Yin, X.; Zhang, Y.; Xu, Y. J. One-Pot, High-Yield Synthesis of One-Dimensional ZnO Nanorods with Well-Defined Morphology as a Highly Selective Photocatalyst. *RSC Adv.* **2013**, *3* (17), 5956−5965.
(35) Zhou, H.; Wang, H.; Zheng, K.; Gu, Z.; Wu, Z.; Tian, X. Aluminum-Doped Zinc Oxide Nanoparticles with Tunable near-Infrared Absorption/Reflectance by a Simple Solvothermal Process. *RSC Adv.* **2014**, *4* (81), 42758−42763.
(36) Ghiloufi, I.; Ghoul, J. El; Modwi, A.; Mir, L. El. Ga-Doped ZnO for Adsorption of Heavy Metals from Aqueous Solution. *Mater. Sci. Semicond. Process.* **2016**, *42* (3), 102−106.
(37) Cao, D.; Gong, S.; Shu, X.; Zhu, D.; Liang, S. Preparation of ZnO Nanoparticles with High Dispersibility Based on Oriented Attachment (OA) Process. *Nanoscale Res. Lett.* **2019**, *14* (1), 210.
(38) Xu, L.; Hu, Y. L.; Pelligra, C.; Chen, C. H.; Jin, L.; Huang, H.; Sithambaram, S.; Aindow, M.; Joesten, R.; Suib, S. L. ZnO with Different Morphologies Synthesized by Solvothermal Methods for Enhanced Photocatalytic Activity. *Chem. Mater.* **2009**, *21* (13), 2875−2885.
(39) Mourdikoudis, S.; Pallares, R. M.; Thanh, N. T. K. Characterization Techniques for Nanoparticles: Comparison and Complementarity upon Studying Nanoparticle Properties. *Nanoscale* **2018**, *10* (27), 12871−12934.
(40) Hou, Y.; Mei, Z.; Tang, A.; Liang, H.; Du, X. Surface Plasmon Enhanced Emission From Defects in Gallium Doped ZnO. *Phys. Status Solidi A* **2018**, *215* (11), 1800037.
(41) Ye, J. D.; Gu, S. L.; Qin, F.; Zhu, S. M.; Liu, S. M.; Zhou, X.; Liu, W.; Hu, L. Q.; Zhang, R.; Shi, Y.; Zheng, Y. D. Correlation between Green Luminescence and Morphology Evolution of ZnO Films. *Appl. Phys. A: Mater. Sci. Process.* **2005**, *81* (4), 759−762.
(42) Ahn, C. H.; Kim, Y. Y.; Kim, D. C.; Mohanta, S. K.; Cho, H. K. A Comparative Analysis of Deep Level Emission in ZnO Layers Deposited by Various Methods. *J. Appl. Phys.* **2009**, *105* (1), 013502.
(43) Zeng, H.; Duan, G.; Li, Y.; Yang, S.; Xu, X.; Cai, W. Blue Luminescence of ZnO Nanoparticles Based on Non-Equilibrium Processes: Defect Origins and Emission Controls. *Adv. Funct. Mater.* **2010**, *20* (4), 561−572.
(44) Alvi, N. H.; Ul Hasan, K.; Nur, O.; Willander, M. The Origin of the Red Emission in N-Zno Nanotubes/p-Gan White Light Emitting Diodes. *Nanoscale Res. Lett.* **2011**, *6* (1), 130.
(45) Bandopadhyay, K.; Mitra, J. Zn Interstitials and O Vacancies Responsible for N-Type ZnO: What Do the Emission Spectra Reveal? *RSC Adv.* **2015**, *5* (30), 23540−23547.
(46) Giau, V. V.; Park, Y. H.; Shim, K. H.; Son, S. W.; An, S. S. A. Dynamic Changes of Protein Corona Compositions on the Surface of Zinc Oxide Nanoparticle in Cell Culture Media. *Front. Chem. Sci. Eng.* **2019**, *13* (1), 90−97.
(47) Panigrahi, S.; Bera, A.; Basak, D. Ordered Dispersion of ZnO Quantum Dots in SiO2Matrix and Its Strong Emission Properties. *J. Colloid Interface Sci.* **2011**, *353* (1), 30−38.

https://doi.org/10.1021/acsanm.1c02197
ACS Appl. Nano Mater. XXXX, XXX, XXX−XXX

(48) Arooj, S.; Xu, T.; Hou, X.; Wang, Y.; Tong, J.; Chu, R.; Liu, B. Green Emission of Indium Oxide: Via Hydrogen Treatment. *RSC Adv.* **2018**, *8* (21), 11828−11833.
(49) Lee, S. Y.; Matsubara, T.; Numata, D.; Serizawa, A. Facile Synthesis of Potassium-Doped Titanium Oxide Nanostructure (KTiOxs)/AlO(OH) Composites for Enhanced Photocatalytic Performance. *Catalysts* **2021**, *11*, 548.
(50) Dulda, A. Morphology Controlled Synthesis of α -GaO(OH) Nanoparticles: Thermal Conversion to Ga2O3 and Photocatalytic Properties. *Adv. Mater. Sci. Eng.* **2016**, *2016*, 1.
(51) Mass, J.; Bhattacharya, P.; Katiyar, R. S. Effect of High Substrate Temperature on Al-Doped ZnO Thin Films Grown by Pulsed Laser Deposition. *Mater. Sci. Eng., B* **2003**, *103* (1), 9−15.
(52) Ramana, C. V.; Rubio, E. J.; Barraza, C. D.; Miranda Gallardo, A.; McPeak, S.; Kotru, S.; Grant, J. T. Chemical Bonding, Optical Constants, and Electrical Resistivity of Sputter-Deposited Gallium Oxide Thin Films. *J. Appl. Phys.* **2014**, *115* (4), 043508.
(53) Choi, D.; Hong, S. J.; Son, Y. Characteristics of Indium Tin Oxide (ITO) Nanoparticles Recovered by Lift-off Method from TFT-LCD Panel Scraps. *Materials* **2014**, *7* (12), 7662−7669.
(54) Pandurangan, M.; Kim, D. H. In Vitro Toxicity of Zinc Oxide Nanoparticles: A Review. *J. Nanopart. Res.* **2015**, *17* (3), 158.
(55) Khashan, K. S.; Sulaiman, G. M.; Hussain, S. A.; Marzoog, T. R.; Jabir, M. S. Synthesis, Characterization and Evaluation of Anti-Bacterial, Anti-Parasitic and Anti-Cancer Activities of Aluminum-Doped Zinc Oxide Nanoparticles. *J. Inorg. Organomet. Polym. Mater.* **2020**, *30* (9), 3677−3693.
(56) Moos, P. J.; Olszewski, K.; Honeggar, M.; Cassidy, P.; Leachman, S.; Woessner, D.; Cutler, N. S.; Veranth, J. M. Responses of Human Cells to ZnO Nanoparticles: A Gene Transcription Study. *Metallomics* **2011**, *3* (11), 1199−1211.
(57) Zhang, Y. N.; Poon, W.; Tavares, A. J.; McGilvray, I. D.; Chan, W. C. W. Nanoparticle-Liver Interactions: Cellular Uptake and Hepatobiliary Elimination. *J. Controlled Release* **2016**, *240*, 332−348.
(58) Wang, J.; Gao, S.; Wang, S.; Xu, Z.; Wei, L. Zinc Oxide Nanoparticles Induce Toxicity in CAL 27 Oral Cancer Cell Lines by Activating PINK1/Parkin-Mediated Mitophagy. *Int. J. Nanomed.* **2018**, *13*, 3441−3450.
(59) Pandurangan, M.; Enkhtaivan, G.; Kim, D. H. Anticancer Studies of Synthesized ZnO Nanoparticles against Human Cervical Carcinoma Cells. *J. Photochem. Photobiol., B* **2016**, *158*, 206−211.
(60) Murdock, R. C.; Braydich-Stolle, L.; Schrand, A. M.; Schlager, J. J.; Hussain, S. M. Characterization of Nanomaterial Dispersion in Solution Prior to in Vitro Exposure Using Dynamic Light Scattering Technique. *Toxicol. Sci.* **2008**, *101* (2), 239−253.
(61) Moon, S. H.; Choi, W. J.; Choi, S. W.; Kim, E. H.; Kim, J.; Lee, J. O.; Kim, S. H. Anti-Cancer Activity of ZnO Chips by Sustained Zinc Ion Release. *Toxicol. Reports* **2016**, *3*, 430−438.
(62) Wang, J.; Lee, J. S.; Kim, D.; Zhu, L. Exploration of Zinc Oxide Nanoparticles as a Multitarget and Multifunctional Anticancer Nanomedicine. *ACS Appl. Mater. Interfaces* **2017**, *9* (46), 39971−39984.
(63) Golombek, S. K.; May, J. N.; Theek, B.; Appold, L.; Drude, N.; Kiessling, F.; Lammers, T. Tumor Targeting via EPR: Strategies to Enhance Patient Responses. *Adv. Drug Delivery Rev.* **2018**, *130*, 17−38.
(64) Wilhelm, S.; Tavares, A. J.; Dai, Q.; Ohta, S.; Audet, J.; Dvorak, H. F.; Chan, W. C. W. Analysis of Nanoparticle Delivery to Tumours. *Nat. Rev. Mater.* **2016**, *1*, 1−12.
(65) Benasutti, H.; Wang, G.; Vu, V. P.; Scheinman, R.; Groman, E.; Saba, L.; Simberg, D. Variability of Complement Response toward Preclinical and Clinical Nanocarriers in the General Population. *Bioconjugate Chem.* **2017**, *28* (11), 2747−2755.
(66) Bisht, G.; Rayamajhi, S. ZnO Nanoparticles: A Promising Anticancer Agent. *Nanobiomedicine* **2016**, *3*, 9.
(67) Hanley, C.; Layne, J.; Punnoose, A.; Reddy, K. M.; Coombs, I.; Coombs, A.; Feris, K.; Wingett, D. Preferential Killing of Cancer Cells and Activated Human T Cells Using ZnO Nanoparticles. *Nanotechnology* **2008**, *19*, 295103.
(68) Puvvada, N.; Rajput, S.; Kumar, B. N. P.; Sarkar, S.; Konar, S.; Brunt, K. R.; Rao, R. R.; Mazumdar, A.; Das, S. K.; Basu, R.; Fisher, P. B.; Mandal, M.; Pathak, A. Novel ZnO Hollow-Nanocarriers Containing Paclitaxel Targeting Folate-Receptors in a Malignant PH-Microenvironment for Effective Monitoring and Promoting Breast Tumor Regression. *Sci. Rep.* **2015**, *5*, 1−15.
(69) Hu, Z.; Li, J.; Li, C.; Zhao, S.; Li, N.; Wang, Y.; Wei, F.; Chen, L.; Huang, Y. Folic Acid-Conjugated Graphene-ZnO Nanohybrid for Targeting Photodynamic Therapy under Visible Light Irradiation. *J. Mater. Chem. B* **2013**, *1* (38), 5003−5013.
(70) Navale, G. R.; Thripuranthaka, M.; Late, D. J.; Shinde, S. S. Antimicrobial Activity of ZnO Nanoparticles against Pathogenic Bacteria and Fungi. *JSM Nanotechnol. Nanomedicine* **2015**, *3* (1), 1033.

https://doi.org/10.1021/acsanm.1c02197
ACS Appl. Nano Mater. XXXX, XXX, XXX−XXX